



HAL
open science

Modelling quenching mechanisms of disordered molecular systems in the presence of molecular aggregates

Giacomo Fanciullo, Irene Conti, Pascal Didier, Andrey Klymchenko, Jérémie Leonard, Marco Garavelli, Ivan Rivalta

► **To cite this version:**

Giacomo Fanciullo, Irene Conti, Pascal Didier, Andrey Klymchenko, Jérémie Leonard, et al.. Modelling quenching mechanisms of disordered molecular systems in the presence of molecular aggregates. *Physical Chemistry Chemical Physics*, 2021, 24 (3), pp.1787-1794. 10.1039/D1CP04260B . hal-03818492

HAL Id: hal-03818492

<https://hal.science/hal-03818492>

Submitted on 17 Oct 2022

HAL is a multi-disciplinary open access archive for the deposit and dissemination of scientific research documents, whether they are published or not. The documents may come from teaching and research institutions in France or abroad, or from public or private research centers.

L'archive ouverte pluridisciplinaire **HAL**, est destinée au dépôt et à la diffusion de documents scientifiques de niveau recherche, publiés ou non, émanant des établissements d'enseignement et de recherche français ou étrangers, des laboratoires publics ou privés.

Modelling quenching mechanisms of disordered molecular systems in presence of molecular aggregates.

Received 00th January 20xx,
Accepted 00th January 20xx

DOI: 10.1039/x0xx00000x

Giacomo Fanciullo,^a Pascal Didier,^b Andrey Klymchenko,^b Jérémie Léonard,^c Marco Garavelli^a and Ivan Rivalta*^{a,d}

The exciton density dynamics recorded in time-resolved spectroscopic measurements is a useful tool to recover information on energy transfer (ET) processes that can occur at different timescales, up to the ultrafast regime. Macroscopic models of exciton density decays, involving both direct Förster-like ET and diffusion mechanisms for exciton-exciton annihilation, are largely used to fit time-resolved experimental data but are generally neglecting contribution from molecular aggregates that can work as quenching species. In this work, we introduce a macroscopic model that includes contributions from molecular aggregate quenchers in a disordered molecular system. As an exemplifying case, we considered a homogenous distribution of rhodamine B dyes embedded in organic nanoparticles to set initial parameters of the proposed model. The influence of such model parameters is systematically analysed, showing that the presence of molecular aggregate quenchers can be monitored by evaluating the exciton density long time decays. We showed that the proposed model can be applied to molecular systems with ultrafast decays, and we anticipated that it could be used in future studies for global fitting of experimental data with potential support from first-principles simulations.

Introduction

The theoretical modelling of the exciton density dynamics allows to shed light on the photophysical processes happening within photoactive materials, such as those employed in the development of artificial light-harvesting systems and organic light emitting diodes. Typical materials of interest are those based on conjugated polymers in the solid phase [1-4], where structural defects localize the excited states into small portions of the polymer chain acting as independent dyes, but several studies have been performed on aggregates in the solid phase [5,6], thin solid films of organic dyes [7-8] and on the so-called host-guest systems, where organic dyes are spatially distributed within polymeric hosts in form of films [9,10] or nanoparticles [11,12]. If dyes are weakly interacting, one can assume excitons localized on individual dyes and thus able to

move through the dye distribution. This exciton mobility can be described by invoking an incoherent energy transfer (ET) hopping mechanism, which can be successfully described by the Förster theory of the ET [13,14]. In Förster model, the timescale governing the donor-acceptor ET is strictly dictated by the radiative (or fluorescence) lifetime of the donor molecule. Typical lifetimes for fluorophores range within the nanosecond scale, but several ETs have been experimentally observed to happen also on the picosecond [2,15] and ultrafast femtosecond [16] timescales.

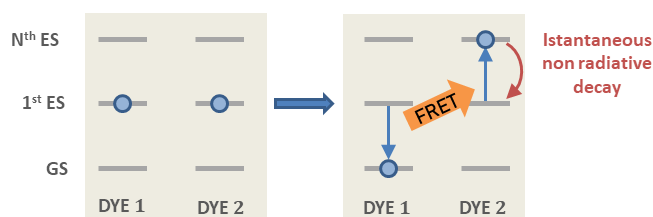


Figure 1. The mechanism for exciton-exciton annihilation (EEA). The excitation is transferred between two excited dyes (DYE 1 and 2), leading to an excited state absorption (to the N^{th} excited state) in one dye (DYE 2) and to a relaxation to ground state in the other one (DYE 1). The N^{th} high-lying is expected to fastly decay non-radiatively to the first excited state, leading to the annihilation of one excitation (i.e. that of DYE 1).

^a Dipartimento di Chimica Industriale "Toso Montanari", ALMA MATER STUDIUM, Università di Bologna, Viale del Risorgimento 4, 40126 Bologna, Italia

^b Laboratoire de Bioimagerie et Pathologies, UMR 7021 CNRS, Université de Strasbourg, 74 Route du Rhin, 67401 Illkirch, France

^c Université de Strasbourg, CNRS, Institut de Physique et Chimie des Matériaux de Strasbourg, UMR 7504, F-67000 Strasbourg, France

^d Université de Lyon, École Normale Supérieure de Lyon, Université Lyon 1, CNRS UMR 5182, Laboratoire de Chimie, 46 allée d'Italie, F69364 Lyon, France

Electronic Supplementary Information (ESI) available: [details of any supplementary information available should be included here]. See DOI: 10.1039/x0xx00000x

Other than the exciton mobility, the ET can be responsible for quenching mechanisms which remove excitations from the system. A quenching process driven by ET is the so-called exciton-exciton annihilation (EEA), which leads to a loss of excitations from the system due to the interaction between the excited states of two molecular dyes in spatial proximity. As shown in Figure 1, the EEA occurs when an excited dye transfers its excitation energy to another excited dye, promoting it to a higher excited state while returning to its ground state. The lifetime of higher excited states is usually very small due fast non-radiative internal conversion processes which are likely to relax back the dye to its first excited state. Since the higher excited state can be rapidly depopulated via non-radiative mechanisms, the whole process describes a fast loss of excitation from the system.

The time evolution of the exciton density, which can also occur in an ultrafast time scale [17], is generally studied by the mean of transient absorption [2,3,5-9,17] or photoluminescence decays [10,18,19] measurements. The recorded, time-resolved signal is proportional to the time-dependent exciton density within the sample, and the proportionality constant is usually recovered by determining the number of absorbing dyes, i.e. their excitation probability under illumination by the light pulse used. In photoluminescence decays experiments, straightforward evidence for the presence of EEA is the acceleration of the fluorescence signal decay upon increasing the excitation power: since powerful irradiations excite a higher number of dyes, excited dyes become closer in space thereby increasing their annihilation probability. Still, the decay of the excitation density can be also affected by other competing quenching phenomena, such as the ET to non-fluorescent aggregates of dyes that is often neglected, while the role of molecular aggregation in the photophysical properties of optical systems is attracting increasing attention. For instance, the effect of the aggregation has been extensively studied in the application of the rhodamine B based dyes employed in the building of artificial light harvesting nanosystems [11,20]. Rhodamine B aggregates are known to be fluorescence quenchers [21,22] and it has been demonstrated that the use of bulky hydrophobic counterions efficiently prevent aggregation [23,24]. Previous theoretical investigations suggested that such quenching mechanism could be due to the fact that rhodamine B dimers (with H-type aggregation) feature dark charge-transfer excited states very close in energy to the bright states, allowing for internal conversion processes that provide suitable paths for non-radiative decays. [22]

Reliable theoretical simulations of the fluorescence decay acceleration in presence of EEA can thus provide essential information on the spatial distribution of molecular excitations and on the concomitant role of molecular aggregation on photoactive materials. The theoretical simulation of the time evolution of the exciton density in presence of EEA could be derived through a microscopic description based on the quantum master equation formalism [25], which gives the time evolution of the population of each individual dye, but this level of theory requires a deep knowledge of the dye distribution, in particular of the distances between dyes and their relative orientation. In fact, such approach has been applied to conjugated polymers for which simplified but

reliable spatial models are available [26-28], but for disordered systems detailed information about the structure cannot be straightforwardly achieved. A simpler level of description invokes for a macroscopic description of the exciton density by strictly assuming a homogeneous distribution of dyes. Exclusively in this framework, the exciton density $n(t)$ (quantifying the number of excited dyes per volume unit) in presence of EEA can be described using the following equation:

$$\frac{dn(t)}{dt} = -\frac{1}{\tau}n(t) - \frac{1}{2}k_{EEA}(t)n(t)^2 \quad (1)$$

Here, the first term describes the decay due to the excited state dye lifetime, with lifetime τ comprising both radiative and non-radiative processes, while the second describes the decay due to EEA. As shown in Figure 2, three different models have been developed to express the rate constant k_{EEA} .

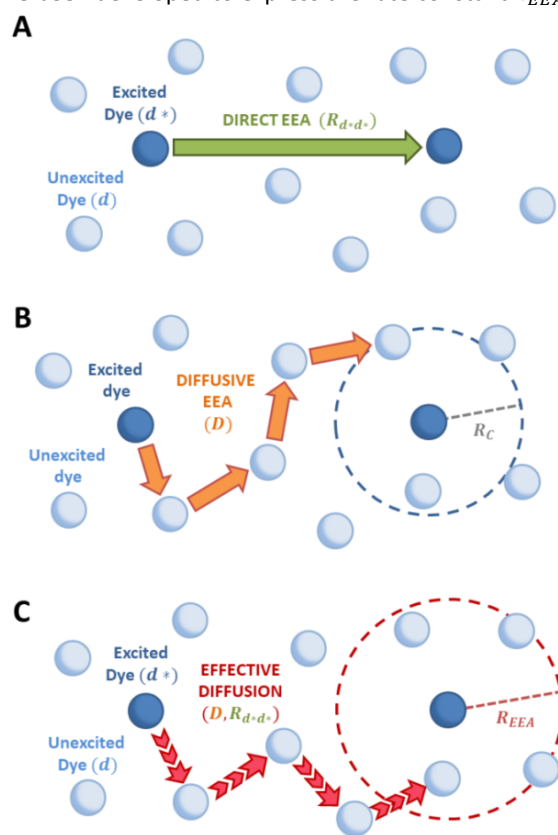


Figure 2. Schematic representation of possible EEA mechanisms. A) The direct mechanism follows the Förster theory and the ET is governed by the Förster radius R_{d,d^*} . B) The diffusive mechanism involves a sequence of energy hops moving from the excited dye through the unexcited ones described by a diffusion coefficient D , while the EEA is assumed to take place when the exciton enters the contact sphere defined by the contact radius R_C . C) The model by Gösele et al. (in the predominant direct mechanism regime as proposed in Ref. 8) describes the combined effect of both direct and diffusive mechanisms as an effective diffusive mechanism driven by the usual diffusion coefficient D but governed by a new contact radius R_{EEA} , which in turns depends on both the Förster radius R_{d,d^*} and D .

In the “direct mechanism” model, the EEA is assumed to happen as described by the Förster ET theory (Figure 2A), and the rate constant takes the form originally derived by Förster [13] for a generic donor-acceptor pair:

$$k_{EEA}(t) = \frac{2}{3}\pi R_{d^*d}^3 \sqrt{\frac{\pi}{\tau_{rad} t}} \quad (2)$$

where R_{d^*d} is the Förster radius related to the ET between two excited dyes and τ_{rad} is the fluorescence lifetime of the dye. The $t^{-1/2}$ time dependence indicates the fact that excitations in close proximity annihilate firstly, thus reducing with time the probability of having annihilation events.

In the “diffusive mechanism” model, the excitations are allowed to diffuse through dyes, and the EEA is assumed to take place when two excitations reach a certain contact radius R_c (figure 2b). The rate constant takes the form derived for the generic problem of a diffusing particle captured by an immobile capturing center [29]:

$$k_{EEA}(t) = 8\pi D R_c \left(1 + \frac{R_c}{\sqrt{2\pi D t}}\right) \quad (3)$$

Here, D is the diffusion coefficient describing the excitation mobility within the dye network. If we consider excitations moving in the dye network through a Förster hopping mechanism, the diffusion coefficient may be expressed as [30-33]

$$D = \eta \frac{R_{d^*d}^6}{\tau_{rad}} \left(\frac{4}{3}\pi C_d\right)^{4/3} \quad (4)$$

Where R_{d^*d} is the Förster radius related to the ET between an excited and a relaxed dye, C_d is the dye concentration and $\eta = 0.43$ is a factor accounting for the homogeneous distribution of dyes. The capability of eq.(4) to correctly estimate the diffusion coefficient has been analysed in detail by Colby et al [10], showing that its successful application could be compromised by several conditions such as the dye aggregation, the breakdown of the dipole-dipole interaction to describe the electronic coupling or the anomalous diffusion driven by energetic and orientational disorder. In this work, we will assume a framework in which the expression for the diffusion coefficient given by eq.(4) is valid and the dye aggregation contribution can be treated separately (as the aggregates, acting as quenchers, will be not directly involved in the diffusion processes). Eq. (4), in fact, allows for an interesting parametrization of the diffusive-related phenomena by simply introducing the additional Förster radius R_{d^*q} .

Gösele et. al. [34-37] derived equations for the rate constant considering both direct and diffuse mechanisms, as depicted in Figure 2A and 2B, and their results have been re-obtained starting from a more sophisticated model by Jang et al [38]. They distinguish two different regimes, having one among the

diffusive or the direct ET mechanisms as predominant. For each regime, they also consider two limiting temporal scales: the short-times scale, where only one mechanism is assumed to rapidly start, and the long-times scale, where a stationary regime is assumed, i.e. the probability of having a decay due to both mechanisms is considered constant in time. The authors proposed that an approximate form for the global rate constants (one for each regime) should be obtained by simply summing the expressions for the two temporal scales. In the predominant diffusion regime, at short times only the diffusive mechanism is assumed to happen, and the global rate equation takes the same form of the pure diffusive case, eq.(3). In this work we will focus on the predominant direct ET regime (see Figure 2C), which has been already suggested for simulations of the exciton density decays [9]. In this regime, the diffusion is assumed not to be started yet at short times, and the rate constant $k_{EEA}^{short}(t)$ becomes the same of the Förster model in eq.(2), while at long times the rate constant takes the form

$$k_{EEA}^{long} = 4\pi D 0.676 \left(\frac{R_{d^*d}^6}{\tau_{rad} D}\right)^{1/4} \quad (5)$$

It is worth noting that although the direct mechanism is predominant, for the rate constant exists a dependence on the diffusion coefficient. The global rate constant is finally calculated as

$$k_{EEA}(t) \approx k_{EEA}^{short}(t) + k_{EEA}^{long} \quad (6)$$

which can be rewritten in a compact form as

$$k_{EEA}(t) \approx 4\pi D R_{EEA} \left(1 + \frac{R_{EEA}}{\sqrt{\pi D t}}\right) \quad (7)$$

where a new “annihilation radius” R_{EEA} has been introduced

$$R_{EEA} = 0.676 \left(\frac{R_{d^*d}^6}{\tau_{rad} D}\right)^{1/4} \quad (8)$$

Since the expression obtained for the rate constant has the same form of the diffusive mechanism one, eq.(3), we can consider the combination of the two processes as a new “effective diffusion” process, with a new contact distance equal to the annihilation radius (see Figure 2C).

As mentioned above, it could be the case that EEA is not the only process responsible for the decay of the excitation density: if the system contains intruder quenching species (such as non-fluorescent aggregates of dyes), the ET from excited dyes to these molecular quenchers will act as a new channel for wasting excitations. Once the excitation energy has been transferred to quenchers, they likely do not relax instantaneously but rather feature a non-radiative lifetime, which implies that an excited quencher density evolving in time has to be considered. In this work, the excitation density

time-evolution of a photoactive system involving both the EEA and the dye-to-quencher ET phenomena (with dyes' aggregates as quenchers) is phenomenologically modelled based on the model of Gösele et al. in a regime where the direct ET is the predominant effect. We report a detailed analysis of the effects of the presence of a small amount of quenchers and of the influence of all model parameters used to simulate the exciton density decays in disordered molecular systems. In order to describe the applicability of the model to a realistic system, we consider as a hypothetical case of study the distribution of alkyl rhodamine B dye with bulky counterions within the organic nanoparticles presented in Ref. [11], from which we take some parameters, such as the dye's fluorescence lifetime and concentration. We finally discuss on the usefulness of model for the global fitting of experimental data and its applicability, which should stimulate future developments to obtain model parameters from first-principles simulations.

Results and discussion

The time evolution of the excitation densities for dyes $n_d(t)$ and quenchers $n_q(t)$ (we assume no triplet states population) is described by the following system of coupled equations:

$$\frac{dn_d(t)}{dt} = -\frac{1}{\tau_d}n_d(t) - k_{EEA}(t)n_d(t)^2 - k_Q(t)n_d(t)[n_q^{TOT} - n_q(t)] \quad (9)$$

$$\frac{dn_q(t)}{dt} = -\frac{1}{\tau_q}n_q(t) + k_Q(t)n_d(t)[n_q^{TOT} - n_q(t)]$$

where $n_q^{TOT} - n_q(t)$ is the density of relaxed quenchers expressed in terms of the total concentration of quenchers n_q^{TOT} , and with τ_d and τ_q being the total lifetimes of dye and quencher, respectively (accounting for both non-radiative and radiative processes in the case of the dye).

The ET processes considered in our model are depicted in Figure 3. The rate constants for the EEA are described by eq.s (7) and (8) with a diffusion coefficient given by eq.(4), and similar expressions are considered also for the dye-quencher ET:

$$k_Q(t) = 4\pi D R_q \left(1 + \frac{R_q}{\sqrt{\pi D t}} \right) \quad (10)$$

$$R_Q = 0.676 \left(\frac{R_{d^*q}^6}{\tau_d^{rad} D} \right)^{1/4} \quad (11)$$

In the following, the analysis of parameters affecting the numerical solution of eq.(9) is reported by assuming a slight amount of quenching species within the dye distribution. We consider as reference dye rhodamine B, having a radiative lifetime $\tau_d^{rad} = 4.24$ ns (corresponding to the measured value

for the 0.1% loaded nanoparticles in ref. [20]) with a concentration of $C_d^{TOT} = 0.13$ dyes/nm³ (corresponding to the 30% loaded nanoparticles in ref. [20]). We initially assume the quencher not to exceed 1% of the dye concentration, thus simulating a typical experimental situation in which a residual aggregation persists in the system despite the efforts made to prevent it. We neglect, for simplicity, the possibility of having non-radiative contributions to the lifetime of both dye and quencher. Equations (9) has to be solved imposing certain initial condition, that is the exciton density at the time zero, $n_d(0)$: we consider that immediately after the light pulse that 7% of the total dyes are excited (a population value falling in the typical experimental range [9]), while we assume that no quenchers are initially excited. This assumption is based on the fact that a small amount of aggregates is present in the sample (we generally consider <1% of C_d^{TOT}) and likely their absorption maximum is shifted from that of isolated dyes since, to work as quenchers, a strong electronic coupling has to be present among the monomeric units. The effect of varying the initial values of the exciton density simulates the typical acceleration of the exciton density decay upon power light increase in experiments (an example is provided in the SI, see Figure S1 in section S.1).

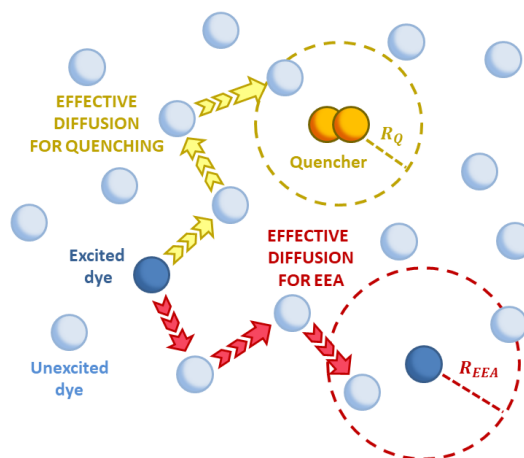


Figure 3. The two possible mechanisms for the exciton loss in presence of both EEA and quenching species (such as dimers in the case of rhodamine B) described by the Gösele model in the predominant direct mechanism regime. The new introduced contact radii R_{EEA} and R_Q depends on the Förster radii $R_{d^*d^*}$ and R_{d^*q} respectively, and depend also on the same diffusion coefficient D .

The following analysis aims highlighting the various effects of the parameters entering our model, emphasizing those features that could allow a straightforward identification of the presence of intruder quenching species. We also explored how much such analysis could depend on the initially chosen values for dye/quencher lifetimes and concentrations, showing the adaptability of our tools to various molecular systems with ET processes occurring at different time scales, from nanoseconds to the ultrafast.

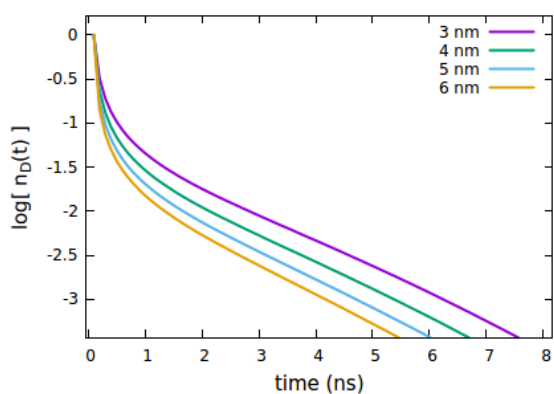


Figure 4. Effect of the R_{d*d^*} radius governing the direct EEA mechanism on the (normalized) exciton density decay. Fixed parameters are: $R_{d*d} = 5$ nm; $R_{d*q} = 2$ nm; $\tau_q = 4$ ns; $C_q = 0.25$ % of C_d^{TOT} ; $n_d(0) = 7$ % of C_d^{TOT} .

First, we consider the effects of the Förster radii R_{d*d} and R_{d*d^*} parameters, governing the exciton mobility through diffusion (influencing both diffusive EEA and diffusive ET to the quenchers) and the direct EEA, respectively. Typical values for Förster radii are up to 8 nm [39], thus we decided to test values within the 3-6 nm range. To highlight the effect of the two EEA processes, the R_{d*q} radius governing the dye-quencher ET and the quencher concentration C_q are set to small values, i.e. 2 nm and 0.25% of C_d^{TOT} respectively. From Figure 4 it is clear that R_{d*d^*} has an influence only on the decays at short time, with the initial decay accelerating upon increasing the radius while leaving unaltered the long times evolution. This result indicates that the EEA events, following the direct mechanism, start immediately after the light pulse and becomes less probable with time, as the spatially closed excitations are depleted through the annihilation.

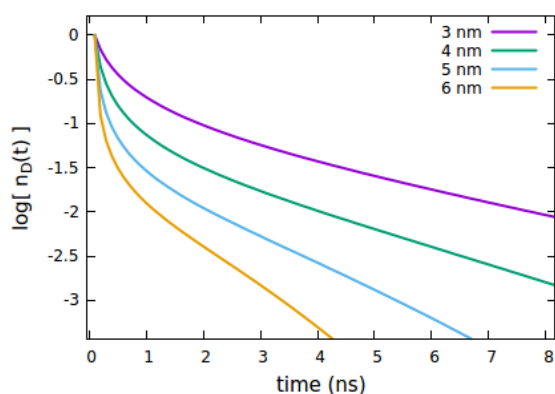


Figure 5. Effect of the R_{d*d} radius governing both EEA and quenching diffusive mechanisms on the (normalized) exciton density decay. Fixed parameters are: $R_{d*d^*} = 4$ nm; $R_{d*q} = 2$ nm; $\tau_q = 4$ ns; $C_q = 0.25$ % of C_d^{TOT} ; $n_d(0) = 7$ % of C_d^{TOT} .

The influence of the R_{d*d} radius is quite different from that of R_{d*d^*} , as clearly shown in Figure 5. Differently from the radius governing the direct EEA, it affects both the short and long

times evolution. While the influence on the short times is similar to R_{d*d^*} , here also the long-time decays are accelerating upon increasing the radius.

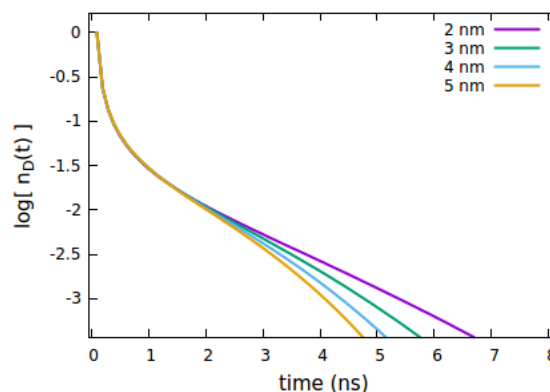


Figure 6. Effect of the R_{d*q} radius governing the direct quenching mechanism on the (normalized) exciton density decay. Fixed parameters are: $R_{d*d^*} = 4$ nm; $R_{d*d} = 5$ nm; $\tau_q = 4$ ns; $C_q = 0.25$ % of C_d^{TOT} ; $n_d(0) = 7$ % of C_d^{TOT} .

We now consider the effect of the parameters related to the quencher species, i.e. its concentration C_q , Förster radius R_{d*q} and radiative lifetime τ_d^{rad} , as reported in Figures 6, 7 and 8A, respectively. It is evident that when the quencher is present in a small amount, its influence can affect the long times evolution only, since the few quencher molecules are very far from the majority of excited dyes and then a certain time has to pass to allow excitations to diffuse towards them. Since this specific (isolated) effect on the long-time evolution cannot be obtained by varying the parameters related to the EEA only, it represents a straightforward signature for the presence of intruder quenching species. Notably, all the trends described above involving an initial amount of excited dyes ($n_d(0) = 7$ % of the C_d^{TOT}), i.e. Figures 2-7, are preserved when such initial (fixed) parameter is significantly increased (see Figures S2-S7 in section S.2 of the SI, for trends with $n_d(0) = 25$ % of the C_d^{TOT}).

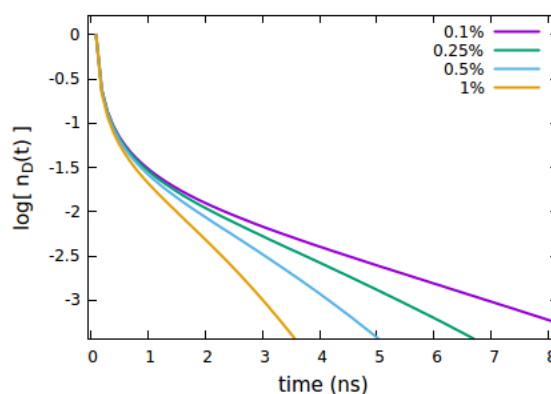


Figure 7. Effect of the quencher concentration C_q (expressed as % of C_d^{TOT}) on the (normalized) exciton density decay. Fixed parameters are: $R_{d*d} = 5$ nm; $R_{d*d^*} = 4$ nm; $R_{d*q} = 2$ nm; $\tau_q = 4$ ns, $C_q = 0.25$ % of C_d^{TOT} ; $n_d(0) = 7$ % of C_d^{TOT} .

It is important to note that the timescale at which the ET processes take place (which in the Förster theory are defined by the molecules' lifetime) does not affect the outcome of the analysis reported above. For instance, as shown in Figure 8, the effect of the quencher lifetime τ_q for ET dynamics in the picosecond and femtosecond timescales (Figures 8B and 8C, respectively) exhibits the same features observed in the nanosecond timescale (Figure 8A). The effects of the other parameters (Förster radii and quencher concentrations discussed in Figures 4-7) are also the same at different timescales, as reported in section S.3 of SI.

The advantage of including quenching species in cases of disordered molecular systems, such as those containing rhodamine B taken as exemplifying case in this work, relies on the fact that a global fitting of experimental decays by using eq.(9) could demonstrate and eventually quantify the presence of intruder quenchers due to aggregation phenomena. It is worth mentioning that we performed some preliminary tests on real experimental data, observing that the model is able to well fit fluorescence decays when fixing up to two parameters in the proposed model. Clearly, such ability of the model to fit experimental data has to be ascribed to its very high flexibility, originating from the large number of free parameters fitted, including the R_{d*d} and R_{d*d*} Förster radii (governing the diffusive and direct mechanism of ET processes among dyes, respectively) and the three parameters related to the quencher, i.e. its lifetime τ_q , concentration C_q and R_{d*q} Förster radius.

Thus, to make applications of our model bringing real physical information, one has to be able to experimentally and/or theoretically determine the highest number of them. The R_{d*d} can be straightforwardly obtained from the overlap between the steady state absorption and emission spectra of the dye [14,39]. The R_{d*d*} Förster radius could be obtained from the transition absorption spectroscopy by isolating the excited state absorptions contribution and calculating the overlap with the emission spectrum of the dye [9,40]. This is less straightforward than obtaining R_{d*d} since excited state absorptions often overlap with ground state bleaching and stimulated emission signals. In this context, advanced simulations of nonlinear electronic spectroscopy from first-principles, such those developed in our group in the recent years [41-45], would be of great support to apply the presented model to real systems. Still, getting reliable deconvolution of transient absorption spectra into specific (overlapping) signals is a very challenging task also from a theoretical point of view, since signal lineshapes are difficult to simulate quantitatively.[42] Finally, regarding parameters associated to the dye aggregates (working as quenchers in our model), first-principles simulations would also be crucial to estimate the R_{d*q} Förster radius, especially if such aggregates cannot be isolated and their absorption spectra recorded. Using structural models of these aggregates, indeed, absorption and emission spectra could be simulated and their

Förster radius thus estimated. In such a way, one could restrict the set of fitting parameters in our model to the quenchers' concentration and lifetime only, providing fundamental insights into the role of aggregation in the photophysical properties of photo-responsive molecular materials.

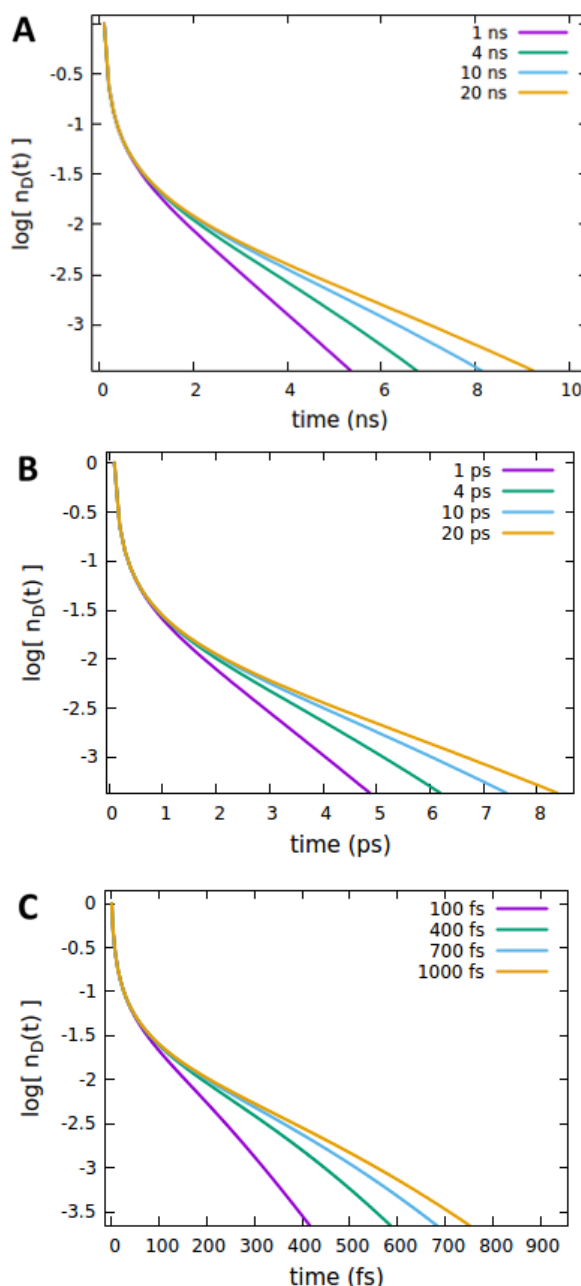


Figure 8. The effect of the quencher lifetime τ_q on the (normalized) exciton density decay considering different timescales for the dye lifetime τ_d , including (A) nanosecond ($\tau_d = 4.242$ ns), (B) picosecond ($\tau_d = 4$ ps), and (C) femtosecond ($\tau_d = 400$ fs) timescales. Fixed parameters are: $R_{d*d} = 5$ nm; $R_{d*d*} = 4$ nm; $R_{d*q} = 2$ nm; $C_q = 0.25$ % of C_d^{TOT} ; $n_d(0) = 7$ % of C_d^{TOT} .

Materials and methods

The system of coupled equations (9) has been solved numerically by means of an in-house Python code employing the *scipy.integrate* package, available upon request to the authors. The rhodamine B dye assemblies in polymeric nanoparticles of [20] have been used as exemplifying case for a disordered molecular system. We considered particles with 45 nm diameter and 30% w/w dye loading. From the average number of rhodamine B molecules per particles reported in [20], we calculated the dye concentration C_d^{TOT} . For the total lifetime τ_d , we considered the value measured for the nanoparticles with the lowest loading (0.1% w/w) because in such a diluted sample a negligible aggregation is expected, and the measured lifetime should be representative for that of isolated dyes. The radiative lifetime τ_d^{rad} has been calculated from the fluorescence quantum yield Φ of the low-loaded nanoparticles through the relation $\Phi = \tau_d / \tau_d^{rad}$.

Conclusions

The exciton density dynamics in photoactive materials is significantly affected by the possibility of having energy transfer (ET) phenomena and the combined use of time-resolved spectroscopy and theoretical modelling has become a widely used tool to recover fundamental information on the type and on the extent of ET processes. When the photoactive system is composed of a uniform distribution of donors and acceptors, simple macroscopic models can be exploited to describe the exciton density dynamics. Such macroscopic models, involving both direct (Förster-like) and diffusive (with ET described by classical diffusion) ET mechanisms, have been successfully applied to describe the influence of exciton-exciton annihilation (EEA) on the exciton density dynamics, but they usually neglect any other quenching phenomena competing with EEA. One of these phenomena that is attracting significant attention is the formation of dye aggregates acting as fluorescence quenchers (e.g. rhodamine B and derivatives).

In this work, we proposed a macroscopic model to simulate exciton density dynamics in disordered molecular systems where both direct (Förster-like) and diffusive (via classical diffusion) ET mechanisms are involved, and allowing both exciton-exciton annihilation (EEA) and ET to molecular aggregates as possible quenching mechanisms. To explore the applicability of the model on a realistic system, we considered as study case a homogeneous system in which rhodamine B dyes are embedded in polymeric nanoparticles. We performed a systematic analysis on the role of various parameters, including the Förster radius R_{d^*a} that is used to express the dye excitation diffusion coefficient, the Förster radii $R_{d^*d^*}$ and R_{d^*q} governing quenching mechanisms via the EEA among dyes and dye-to-aggregate ET, respectively, and the aggregate quencher's concentration and lifetime. The results suggested that while the R_{d^*a} and $R_{d^*d^*}$ inevitably affect the short-time behaviour of the decay, the parameters related to the quenchers have an influence only on the long-time decays, providing a fingerprint of aggregation effects on exciton

density dynamics. Moreover, we showed that the effect of a small amount of quencher exhibits always the same features, independently from the power of the light source experimentally used and, more importantly, independently from the ET timescales, including the case of ultrafast dynamics. The overall outcome indicates that the application of our model to real cases could allow straightforward identification of quenching effects arising from molecular aggregates. This could be achieved by global fitting analysis of experimental data that, however, could be compromised by an extreme flexibility of the model, in case of too many parameters are set free. Thus, we envisioned that experimental determination of some of the model parameters could be supported by first-principles simulations. In particular, when the experimental determination is very challenging, as for parameters of the quenching aggregated species or those derived from deconvolution of time-resolved electronic spectra of the dye, first-principles estimates of parameters could enter in our model, potentially providing unique information on the role of molecular aggregation on the photophysical properties of photoactive materials.

Author Contributions

We strongly encourage authors to include author contributions and recommend using [CRediT](#) for standardised contribution descriptions. Please refer to our general [author guidelines](#) for more information about authorship.

Conflicts of interest

In accordance with our policy on [Conflicts of interest](#) please ensure that a conflicts of interest statement is included in your manuscript here. Please note that this statement is required for all submitted manuscripts. If no conflicts exist, please state that "There are no conflicts to declare".

Acknowledgements

The acknowledgements come at the end of an article after the conclusions and before the notes and references.

Notes and references

- 1 Y. Jiag, J. McNeill, *Chem. Rev.*, 2017, **117**, 838.
- 2 A. Dogariu, R. Gupta, A. J. Heeger, H. Wang, *Synthetic Metals*, 1999, **100**, 95
- 3 S. M. King, D. Dai, C. Rothe, A. P. Monkman, *Phys. Rev. B*, 2007, **76**, 085204.
- 4 A. J. Lewis, A. Ruseckas, O.P.M. Gaudin, G.R. Webster, P.L. Burn, I.D.W. Samuel, *Organic Electronics*, 2006, **7**, 452.
- 5 G. de Miguel, M. Ziółek, M. Zitnan, J. A. Organero, S. S. Pandey, S. Hayase, A. Douhal, *J. Phys. Chem. C*, 2012, **116**, 9379
- 6 H. Marciniak, X.-Q. Li, F. Würthner, S. Lochbrunner, *J. Phys. Chem. A*, 2011, **115**, 648.
- 7 S. Chandrabose, K. Chen, A. J. Barker, J. J. Sutton, S. K. K. Prasad, J. Zhu, J. Zhou, K. C. Gordon, Z. Xie, X. Zhan, J. M. Hodgkiss, *JACS*, 2019, **141**, 6922.

- 8 H. Marciniak, I. Pugliesi, B. Nickel, S. Lochbrunner, *Phys. Rev. B*, 2009, **79**, 235318
- 9 F. Fennel, S. Lochbrunner, *Phys. Rev. B*, 2015, **92**, 140301.
- 10 K. A. Colby, J. J. Burdett, R. F. Frisbee, L. Zhu, R. J. Dillon, C. J. Bardeen, *J. Phys. Chem. A*, 2010, **114**, 3471–3482.
- 11 A. Reisch, P. Didier, L. Richert, S. Oncul, Y. Arntz, Y. Mély, A. S. Klymchenko, *Nat. Commun.*, 2014, **5**, 4089.
- 12 S. Bhattacharyya, B. Jana, A. Patra, *Chem. Phys. Chem.*, 2015, **16**, 796.
- 13 T. Förster, *Ann. Phys.*, 1948, **2**, 55.
- 14 G. D. Scholes, *Annu. Rev. Phys. Chem.*, 2003, **54**, 57.
- 15 D. Bai, A. C. Benniston, J. Hagon, H. Lemmetyinen, N. V. Tkachenko, W. Clegg, R. W. Harrington, *Phys. Chem. Chem. Phys.*, 2012, **14**, 4447.
- 16 L. J. Patalag, J. Hoche, M. Holzapfel, A. Schmiedel, R. Mitric, C. Lambert, D. B. Werz, *J. Am. Chem. Soc.*, 2021, **143**, 7414.
- 17 E. Engel, K. Leo, M. Hoffmann, *Chem. Phys.*, 2006, **325**, 170.
- 18 W. Staroske, M. Pfeiffer, K. Leo, M. Hoffmann, *Phys. Rev. Lett.*, 2007, **98**, 197402.
- 19 M. Hasan, A. Shukla, V. Ahmad, J. Sibus, F. Bencheikh, S. K. M. McGregor, M. Mamada, C. Adachi, S.-C. Lo, E. B. Namadas, *Adv. Funct. Mater.* 2020, **30**, 2000580.
- 20 K. Trofymchuk, A. Reisch, P. Didier, F. Fras, P. Gilliot, Y. Mely, A. S. Klymchenko, *Nat. Photonics*, 2017, **11**, 657.
- 21 F. Arbeloa, P. Ojeda, and I. Arbeloa, *Chem. Phys. Lett.*, 1988, **148**, 253.
- 22 D. Setiawan, A. Kazaryan, M.A. Martoprawiro, and M. Filatov, *Phys. Chem. Chem. Phys.*, 2010, **12**, 11238.
- 23 I. Shulov, S. Oncul, A. Reisch, Y. Arntz, M. Collot, Y. Mely, A. S. Klymchenko, *Nanoscale*, 2015, **7**, 18198.
- 24 B. Andreiuk, A. Reisch, E. Bernhardt, A. S. Klymchenko, *Chem. Asian J.*, 2019, **14**, 836.
- 25 V. May - *J. Chem. Phys.* 2014, **140**, 054103.
- 26 K. Hader, V. May, C. Lambert, V. Engel, *Phys. Chem. Chem. Phys.*, 2016, **18**, 13368.
- 27 K. Hader, C. Consani, T. Brixner, V. Engel, *Phys. Chem. Chem. Phys.*, 2017, **19**, 31989.
- 28 L. Wang, V. May, *Phys. Rev. B*, 2016, **94**, 195413.
- 29 R. C. Powell, Z. G. Soos, *J. Lumin.*, 1975, **11**, 1.
- 30 S. W. Haan, R. Zwanzig, *J. Chem. Phys.* 1978, **68**, 1879.
- 31 C. R. Gochanour, H. C. Andersen, M. D. Fayer, *J. Chem. Phys.* 1979, **70**, 4254.
- 32 R. F. Loring, H. C. Andersen, M. D. Fayer, *J. Chem. Phys.* 1982, **76**, 2015.
- 33 P. T. Rieger, S. P. Palese, R. J. D. Miller, *J. Chem. Phys.* 1997, **221**, 85.
- 34 U. Gösele, M. Hauser, U. K. A. Klein, R. Frey, *Chem. Phys. Lett.*, 1975, **34**, 519.
- 35 U. Gösele, M. Hauser, U. K. A. Klein, *Z. Physik. Chem. Neue Folge* 1975, **99**, 81.
- 36 K. A. Klein, R. Fray, M. Hauser - *Chem. Phys. Lett.* 1976, **41**, 139-142.
- 37 U. Gosele, *Spectrosc. Lett.* - 1978, **11**, 445.
- 38 S. Jang, K. J. Shin, S. Lee, *J. Chem. Phys.* 1995, **102**, 815.
- 39 I. Medintz, N. Hildebrandt (eds), *FRET - Förster Resonance Energy Transfer*, 2014, Wiley-VHC.
- 40 D. Nettle, D. Haenni, S. Maillot, M. Gueye, A. Barth, V. Hirschfeld, C. G. Hübner, J. Léonard, B. Schuler, *Phys. Chem. Chem. Phys.*, 2015, **17**, 32304.
- 41 V. K. Jaiswal, J. Segarra-Martí, M. Marazzi, E. Zvereva, X. Assfeld, A. Monari, M. Garavelli, I. Rivalta, *Phys. Chem. Chem. Phys.*, 2020, **22**, 15496.
- 42 J. Segarra-Martí, F. Segatta, T. A. Mackenzie, A. Nenov, I. Rivalta, M. J. Bearpark, M. Garavelli, *Faraday Discuss.*, 2020, **221**, 219.
- 43 J. Segarra-Martí, S. Mukamel, M. Garavelli, A. Nenov, I. Rivalta (2019) Towards Accurate Simulation of Two-Dimensional Electronic Spectroscopy. In: Buckup T., Léonard J. (eds) *Multidimensional Time-Resolved Spectroscopy*. Topics in Current Chemistry Collections. Springer, Cham.
- 44 E. Zvereva, J. Segarra-Martí, M. Marazzi, J. Brazard, A. Nenov, O. Weingart, J. Léonard, M. Garavelli, I. Rivalta, E. Dumont, X. Assfeld, S. Haacke, A. Monari, *Photochem. Photobiol. Sci.*, 2018, **17**, 323.
- 45 A. Nenov, A. Giussani, B. P. Fingerhut, I. Rivalta E. Dumont, S. Mukamel - M. Garavelli, *Phys. Chem. Chem. Phys.*, 2015, **17**, 30925.